Published in final edited form as:
Exp Hematol. 2011 March ; 39(3): 305–320.e2. doi:10.1016/j.exphem.2010.12.009.

A novel ENU-generated truncation mutation lacking the spectrin-binding and C-terminal regulatory domains of Ank1 models severe hemolytic hereditary spherocytosis

Michael R. Hughes[a,*], **Nicole Anderson**[b,*], **Steven Maltby**[a], **Justin Wong**[a], **Zorana Berberovic**[k], **Connie S. Birkenmeier**[h], **D. James Haddon**[a], **Kamal Garcha**[c], **Ann Flenniken**[k], **Lucy R. Osborne**[d], **S. Lee Adamson**[e,i], **Janet Rossant**[f,l], **Luanne L. Peters**[h], **Mark D. Minden**[b,g,m,n], **Robert F. Paulson**[o], **Chen Wang**[j], **Dwayne L. Barber**[g,n], **Kelly M. McNagny**[a,†], and **William L. Stanford**[b,c,†]

[a]The Biomedical Research Centre, University of British Columbia, Vancouver, BC, Canada

[b]Institute of Medical Science, University of Toronto, Toronto, ON, Canada

[c]Institute of Biomaterials and Biomedical Engineering, University of Toronto, Toronto, ON, Canada

[d]Department of Medicine, University of Toronto, Toronto, ON, Canada

[e]Department of Obstetrics and Gynecology, University of Toronto, Toronto, ON, Canada

[f]Department of Medical Genetics, University of Toronto, Toronto, ON, Canada

[g]Department of Medical Biophysics, Faculty of Medicine, University of Toronto, Toronto, ON, Canada

[h]The Jackson Laboratory, Bar Harbor, Me., USA

[i]Samuel Lunenfeld Research Institute, Toronto, ON, Canada

[j]Mount Sinai Hospital, Toronto, ON, Canada

[k]Toronto Centre for Phenogenomics, Toronto, ON, Canada

[l]Hospital for Sick Children, Toronto, ON, Canada

[m]Princess Margaret Hospital, Toronto, ON, Canada

[n]Ontario Cancer Institute, Toronto, ON, Canada

[o]Pennsylvania State University, State College, Pa., USA

Abstract

Objective—Hereditary spherocytosis (HS) is a heterogeneous group of spontaneously arising and inherited red blood cell disorders ranging from very mild subclinical cases to severe and life-threatening cases, with symptoms linked directly to the severity of the mutation at the molecular

Offprint requests to: William L. Stanford, Ph.D., Institute of Biomaterials and Biomedical Engineering, University of Toronto, 164 College Street, Toronto, ON, M5S 3G9 Canada; william.stanford@utoronto.ca.
*Drs. Hughes and Anderson contributed equally to this work as first coauthors.
†Drs. McNagny and Stanford contributed equally as senior authors.

Conflict of interest disclosure No financial interest/relationships with financial interest relating to the topic of this article have been declared.

Supplementary data associated with this article can be found in the online version at doi:10.1016/j.exphem.2010.12.009

level. We investigated a novel mouse model in which the heterozygotes present with the diagnostic hallmarks of mild HS and surviving homozygotes phenocopy severe hemolytic HS.

Materials and Methods—We used *N*-ethyl-*N*-nitrosourea mutagenesis to generate random point mutations in the mouse genome and a dominant screen to identify mouse models of human hematopoietic disease. Gene mapping of the HS strain revealed a unique in-frame nonsense mutation arising from a single base transversion in exon 27 of *Ank1* (strain designation: *Ank1*^{E924X}). Employing conventional hematopoietic, pathological, biochemical, and cell biology assays, we characterized heterozygous and homozygous *Ank1*^{E924X} mice at the biochemical, cellular, and pathophysiological levels.

Results—Although *Ank1*$^{E924X/E924X}$ red blood cell ghosts lack abundant full-length ankyrin-1 isoforms, N-terminal epitope ankyrin-1 antibodies reveal a band consistent with the theoretical size of a truncated mutant ankyrin-1. Using domain-specific antibodies, we further show that this protein lacks both a spectrin-binding domain and a C-terminal regulatory domain. Finally, using antisera that detect C-terminal residues of the products of alternative *Ank1* transcripts, we find unique immunoreactive bands not observed in red blood cell ghosts from wild-type or *Ank1*^{E924X} heterozygous mice, including a band similar in size to full-length ankyrin-1.

Conclusions—The *Ank1*^{E924X} strain provides a novel tool to study Ank1 and model HS.

As part of a large-scale project to develop new mouse models of human disease [1], we used a nonbiased, forward genetics approach to generate models of inherited blood disorders. We report one such mouse model that recapitulates the hallmarks of human hereditary spherocytosis (HS). HS is a heterogeneous group of spontaneously arising and inherited red blood cell (RBC) disorders endemic in human populations (see Perrotta et al. [2] for review and references therein). In North America and northern Europe, the diagnosed prevalence of HS is approximately 1 in 2000, with disease severity ranging from very mild subclinical cases to severe and life-threatening cases [2]. HS is predominantly caused by defects in the expression, stability, or function of at least one of the erythroid membrane cytoskeleton components, including ankyrin-1, Band 3, α-spectrin, β-spectrin, and protein 4.2 [3]. A mutation in the ankryin-1 gene (*ANK1*) accounts for approximately half of genetically defined cases of HS, except in Japan, where defects in the protein 4.1 gene (*EPB41*) are more common [3]. The known mutations of *ANK1* in human disease cover the entire locus, including insertions and deletions in the promoter regions, 5′ and 3′ untranslated regions, mutations affecting splicing fidelity, and a variety of nonsense and missense substitutions in coding exons (see review by Gallagher [4] and references therein). Most cases of HS associated with *ANK1* mutations are dominantly inherited (~80% to 85%), but cases of de novo mutations and recessive inheritance are known [3]. In many instances of human disease, the primary mutation in the *ANK1* gene affects the expression or stability of other proteins (especially the spectrins) that cooperatively bind ankyrin-1 in complexes required for appropriate function and assembly of the erythrocyte membranous-cytoskeletal network [5,6].

In mice, as in humans, there are three ankyrin genes (*Ank1, Ank2*, and *Ank3*) encoding ankyrin proteins (ankyrin-1, -2, and -3) that act as adaptor structural components linking lipid membranes to the cytoskeleton and stabilizing transmembrane ion channels (for a recent review see Bennett and Healy [7]). Although *ANK1* is also expressed in other hematopoietic cells, skeletal muscle, neurons, and Purkinje cells of the cerebellum, it is primarily known for its structural role in erythrocytes [8–13].

Expression of *Ank1* (and *ANK1* in humans) is subject to extensive transcriptional variability and many splice variants and their products are observed [14,15]. In erythrocytes, the most prominently expressed transcript variants encode isoforms with varying C-terminal residues

[16,17] and these isoforms may have different functional roles. Other common ankyrin-1 variants are tissue-specific, e.g., a muscle-specific promoter and alternative start-site in *Ank1* intron 39 (mouse) yields a 25-kD short ankyrin-1 isoform that associates with the sarcoplasmic reticulum in skeletal muscle [11,12,18] and a similar isoform is detected in humans [13].

Full-length protein isoforms (200–210 kD) of erythroid *Ank1* consist of three major conserved domains, including an N-terminal band 3-binding domain, a central spectrin-binding domain, and a C-terminal regulatory domain containing a death domain motif (for review see Rubtsov and Lopina [19]) (Fig. 1C). Erythroid ankyrin links band 3 (*AE1*), a transmembrane anion exchanger, to the $\alpha_2\beta_2$ spectrin tetramer and thus the RBC cytoskeletal network [20–23]. The functional unit of ankyrin's spectrin binding domain, the ZO-1 and Unc5-like netrin receptor (ZU5) subdomain, is a 105-residue motif that directly binds β-spectrin [22,24]. Although the precise functions of the death and regulatory domains are largely enigmatic, the regulatory domain appears to modify association of ankyrin-1 with the band 3 complex and the RBC cytoskeleton network [25–28]. Thus, as a linchpin linking the band 3 complex to the red cell cytoskeleton, ankyrin-1 confers the red cell membrane with vertical stability and reversible deformability.

In this report, we characterize a new *N*-ethyl-*N*-nitrosourea (ENU)–induced mutation in the mouse ankyrin-1 gene (mutant allele designated *Ank1*^{E924X}). Heterozygous mice have low RBC mean corpuscular volume (MCV), elevated RBC counts, reticulocytosis, reduced eosin-5′-maleimide RBC-labeling intensity, and increased osmotic fragility. These characteristics, taken together, are diagnostic features of HS [2]. Subsequent mapping of the causal mutation revealed a single base transversion in *Ank1* exon 27 causing an immediate, in-frame termination codon. The theoretical protein product of this mutant *Ank1* allele is truncated proximal (38 residues) to the N-terminal end of the ZU5 subdomain and thus eliminates the conserved domain that facilitates association of ankyrin-1 with β-spectrin [22,23] but, presumably, leaves the N-terminal band 3-binding domain intact. The *Ank1*^{E924X} strain represents a novel mutation in *Ank1* leading to truncation of the spectrin binding and regulatory domains without mutant frame residues and is thus distinct from other *Ank1* mutant mouse strains described previously. Although mice homozygous for *Ank1*^{E924X} do not express detectable full-length canonical isoforms of ankyrin-1, using domain-specific antibodies we detect several unique isoforms or degraded ankyrin protein products that may support survival of *Ank1*^{E924X} homozygous mice.

Material and methods

Mice

C57Bl/6J (*B6*), *C3H/HeJ* (*C3H*), and *SvImJ/129* (*129J*) strains were from The Jackson Laboratory (Bar Harbor, ME, USA). All mice were maintained in specific-pathogen–free housing facilities at the Mount Sinai Hospital Research Institute, University of Toronto (Toronto, ON, Canada) or at The Biomedical Research Centre, University of British Columbia (Vancouver, BC, Canada). ENU-mutagenesis and phenotype screening were conducted at the Mount Sinai Hospital Research Institute facility. All animal experiments were conducted in accordance with the ethical guidelines of the Canadian Council on Animal Care with protocols approved by the University of Toronto and University of British Columbia animal care committees.

ENU mutagenesis and dominant phenotype screening

B6 male mice received three intraperitoneal injections of 85 mg/kg ENU (Sigma-Aldrich, Oakville, ON, Canada) [29]. Mutagenized B6 were outcrossed to C3H females and the first-

generation progeny were screened for dominant peripheral blood (PB) phenotypes using an automated blood analyzer (Coulter Ac-T Differential Hematology Analyzer with veterinary software; Beckman-Coulter, Mississauga, ON, Canada). Mice with PB parameters deviating from littermate progeny or nonmutagenized hybrids (B6:129) were selected for heritability testing and genome mapping. Additional details are provided in the Supplementary Methods (online only, available at www.exphem.org).

Nomenclature

In this article, we use the exon and residue numbering scheme of mouse *Ank1* messenger RNA (NM 031158.2, transcript variant 1) and its 1907 residue peptide product ankyrin-1, isoform 1 (NP 112435.2).

Polymerase chain reaction genotyping

Ank1^{E924X} mice were genotyped by multiplex polymerase chain reaction (PCR) using genomic DNA prepared from tail or ear tissue. Details of the PCR genotyping methods are provided in the Supplementary Methods (Supplementary Figure E1; online only, available at www.exphem.org).

RBC phenotype analysis

Osmotic fragility—Freshly collected PB was resuspended in normal saline (0.9% NaCl), washed once, and then resuspended in 5 mL normal saline. One hundred–microliter aliquots were transferred to a 96-well round-bottom plate and the RBCs were pelleted (1200 rpm, room temperature [RT] for 5 minutes) (Eppendorf Centrifuge 5415 R). RBC pellets were gently resuspended in 200 μL salt solutions ranging from 0.1% to 0.9% NaCl (concentrations as shown in Fig. 1D). After 60 minutes at RT, an aliquot of each sample supernatant was transferred to a flat-bottom 96-well plate and the optical density determined at 545 nm (SpectraMAX 190; Molecular Devices, Sunnyvale, CA, USA). The mean corpuscular fragility is defined as the NaCl concentration on the osmotic fragility curve where 50% RBC lysis is achieved (assumes lysis in 0.1% NaCl 5 100%). Assays were performed in duplicate wells for several age- and sex-matched mice per group.

Reticulocyte analysis

To determine PB reticulocyte percent, one drop of blood was immediately suspended in 2 mL PBS and mixed by inversion. Half of this suspension was added to 1 mL thiazole orange (Sigma-Aldrich) freshly prepared working solution consisting of 5 μL thiazole orange stock (10 mg/mL in 100% MeOH) diluted in 50 mL PBS. This suspension was mixed by inversion and then incubated at RT for 30 minutes in the dark. Reticulocyte percentage (thiazole orange–positive erythrocytes) was determined by flow cytometry (FACSCalibur, BD Biosciences, San Jose, CA, USA).

Eosin-5′-maleimide labeling

Freshly collected PB was washed in PBS as mentioned and then resuspended in a solution of eosin-5′-maleimide and incubated in the dark at RT for 1 hour. This suspension was then washed three times with PBS and resuspended in 100 μL PBS containing 2 mM ethylenediamine tetraacetic acid (EDTA) and 2% fetal calf serum (Gibco, Carlsbad, CA, USA) (fluorescence-activated cell sorting [FACS] buffer). The contents were then transferred into 1 mL FACS buffer for analysis by flow cytometry.

Electron microscopy

Scanning electron micrographs (SEM) of fixed red cells (4% paraformaldehyde, 2.5% gluteraldehyde in 0.1 M sodium cacodylate buffer) were obtained using standard protocols, the details of which are provided in the Supplementary Methods (online only, available at www.exphem.org).

Histology

Mice were euthanized by CO_2 inhalation and then tissues were harvested immediately after sacrifice and fixed in 10% neutral buffered formalin or Bouin's fixative (Sigma-Aldrich, Mississauga, ON, Canada). Tissue sections (4 mm) were prepared and stained with hematoxylin and eosin.

In vitro progenitor assays

Single-cell suspensions of bone marrow (BM), spleen, and liver were prepared in Iscove's modified Dulbecco's medium (Gibco) with 5% fetal bovine serum. RBC lysis was performed on BM, splenocytes, liver, and PB using RBC lysis buffer (0.14M NH_4Cl, 0.017M Tris). Cell counts and viability was assessed on a ViCell automated cell counter (Beckman-Coulter). For each assay, three aliquots of 2×10^4 (BM) or 1×10^5 (splenocytes, liver, and PB) cells were mixed with the appropriate methylcellulose media, plated, and grown in humidified chambers at 37°C, 5% CO_2. For all colony-forming unit cell (CFU-C) assays, we used complete methylcellulose media M3434 except for CFU-erythroid (CFU-E) assays (M3334) (Stemcell Technologies Inc., Vancouver, BC, Canada). CFU-C were enumerated after 8 to 10 days based on colony morphology, whereas CFU-E colonies were counted based on benzidine-positive staining and morphology on day 2.

Flow cytometry

After RBC lysis, single-cell suspensions of BM, spleen, liver, and PB were labeled in FACS buffer with fluorescein isothiocyanate (FITC)–conjugated CD71 and phycoerythrin (PE)-conjugated Ter119 or isotype control monoclonal antibodies, PE-conjugated $IgG_{2b,\kappa}$, and FITC–conjugated $IgG_{2a,\kappa}$ (eBioscience, San Diego, CA, USA). Cell population data were collected using Beckman Coulter FC 500 or FACSCalibur (BD Biosciences) flow cytometer instruments and analyzed using FlowJo software (TreeStar Inc., Ashland, OR, USA).

Antibodies

Antibodies raised against ankyrin-1 domain-specific peptides have been described previously [16,17]. Primary antibodies to detect ankyrin-1 (8C3), α-spectrin (H-110), and β-adducin were purchased from Santa Cruz Biotechnology (Santa Cruz, CA, USA) and the band 3 antibody (AE11-A) was from Alpha Diagnostics (San Antonio, TX, USA). The actin antibody (AC40) we used for immunoblotting was from AbCam (Cambridge, MA, USA). Secondary antibodies for Western detection (anti-goat IgG 800CW and anti-rabbit IgG 700) were from LI-COR Biosciences (Lincoln, NE, USA).

RBC ghost protein analysis and immunoblotting

Approximately 350 to 500 μL blood collected by cardiac puncture of mice immediately after sacrifice (CO_2 asphyxiation) was directly resuspended in 5 volumes PBS containing 2 mM EDTA. RBCs were pelleted, washed once with PBS, repelleted, and then resuspended in 10 volumes ice-cold RBC ghost preparation buffer (5 mM sodium phosphate [pH 8], 1 mM EDTA, 100 μM phenylmethylsulfonyl fluoride) and set aside on ice for 30 to 60 minutes with intermittent mixing by inversion. This suspension was divided into microfuge tubes and ghosts were pelleted at maximum speed for 5 minutes at 4°C. The supernatant was aspirated and the pelleted ghosts were washed five times with 1 mL RBC ghost preparation

buffer, repooled, and then filtered through a filter-top FACS tube sieve (Falcon; BD Biosciences) and then resuspended in 200 μL RBC ghost preparation buffer. Total protein concentration was determined by BCA assay (Pierce, Rockford, IL, USA). Equal concentrations of total protein were boiled for 1 minute in sodium dodecyl sulfate sample buffer containing 2-mercaptoethanol and then fractionated by sodium dodecyl sulfate polyacrylamide gel electrophoresis. Gels were either stained directly with Coomassie Blue or transferred to phenylmethylsulfonyl fluoride membrane for Western analysis. Membranes were blocked in 5% bovine serum albumin (in TBST [TBS, 0.02% Tween20]) for at least 1 hour at RT or overnight at 4°C and then probed with the primary antibodies as indicated. After thorough washing with TBST, secondary detection antibodies were used at a 1:15,000 dilution (in TBST) at RT for 45 minutes, after which the membranes were thoroughly washed and reactive bands were detected using the Odyssey system (LI-COR).

Statistical analysis

GraphPad Prism software was used to calculate significance values (p) using two-tailed Student's t-test. The means of two groups were considered significantly different if $p < 0.05$.

Results

A new mouse model of HS generated by ENU mutagenesis

We used ENU mutagenesis to generate novel dominantly inherited mouse strains with PB phenotypes. In one screening strategy, we identified mutants of interest using automated complete blood counts of blood collected from the first-generation (G1) progeny (6–8 weeks old) of *C57Bl/6* (*B6*) mutagenized male mice outcrossed to *C3H/HeJ* (*C3H*) females. Complete blood count parameters were compared to “nonaffected” littermates and parental strains to identify phenodeviants, and these were subsequently outcrossed with *C3H* for heritability testing, genome mapping, and detailed phenotype analysis. Table 1 shows a summary of the dominant screen. Nearly 3400 G1 animals were tested, leading to 88 phenodeviants detected, of which 43 were tested for heritability, and 17 were confirmed heritable. Interestingly, phenodeviants with alterations in white blood cell or platelet counts or in RBC phenotypes were particularly robust, while G1s, which presented with alterations in RBC counts but without any other phenotypes such as MCV or mean cell hemoglobin, routinely failed heritability testing, indicating the importance of using multiple parameters for selecting RBC mutants.

Strain ENU7192 presented with a dominantly inherited RBC phenotype marked by low MCV and mean cell hemoglobin and high RBC count (Fig. 1A). Progeny with these “affected” phenotypes were selected for gene mapping. Backcrossing to C3H/HeJ for several generations (N8–9) proved that the RBC phenotype was dominantly inherited (Table 2) and blood from affected mice revealed an abnormal blood smear with polychromasia, reduced band 3 surface expression, increased RBC osmotic fragility and reticulocytosis (Fig. 1B–E). Using the mapping strategy shown in Figure 2A, we subsequently mapped the causal mutation to a 7.2-Mb region of Chr. 8 (Fig. 2B). Of the fully annotated genes in this region, few are known to be expressed in hematopoietic cells and only one, *Ank1* (ankyrin-1), is highly expressed in the erythroid lineage [16]. Because the phenotype of the affected mice displays the clinical hallmarks of human HS [2,30], including low MCV, reduced 5′-maleimide mean fluorescence intensity, increased osmotic fragility, and reticulocytosis, we selected *Ank1* as the primary mutant gene candidate. Full sequencing of all *Ank1* exons and intron/exon borders identified a point mutation in *Ank1* exon 27 in affected but not unaffected mice (nor the two parental strains). This point mutation (G → T transversion) causes an in-frame nonsense mutation in the gene transcript, introducing a premature termination stop codon in place of glutamate (E) 924 (mouse ankyrin-1, isoform 1)–38

residues N-terminal of the spectrin-binding subdomain (ZU5) (Fig. 2B). We designated this ENU-generated *Ank1* allele *E924X*. *Ank1*^{E924X} is the most 5′ mutation reported in mice, with the other two known mouse *Ank1* mutations, *nb* and *RBC2*, lying in the 3′ region of *Ank1* that encodes the C-terminal regulatory domain [17,31] (Fig. 2B, C).

Ank1^{E924X} homozygous mutant mice display severe hemolytic anemia, profound extramedullary hematopoiesis, and stress erythropoiesis

All of the features of the dominantly inherited RBC phenotype were maintained upon outcrossing *Ank1*^{E924X} heterozygous mice to a *129J* genetic background (data not shown). As *Ank1*$^{E924X/+}$ (Het) hybrid mice age, they also show significantly enlarged spleens compared to wild-type (WT) littermates (spleen indices are Het = 6 [standard deviation {SD} = 1]; WT = 2 [SD = 1]; n = 4, $p << 0.05$]). Although we do not observe live homozygous neonates from intercrosses of heterozygous *Ank1*^{E924X} mice on a C3H/HeJ genetic background (N8–9), we do obtain viable homozygous progeny from intercrosses of an *Ank1*$^{E924X/+}$ hybrid strain (*C3H/HeJ* x *SvImJ/129* [N2]). The frequency of mice surviving to weaning with an *E924X/E924X* genotype is under-represented (11% [n = 42]) with respect to the expected Mendelian inheritance distribution. In contrast, although most *E924X/E924X* embryos late in gestation (E17.5) are pale and underweight (Fig. 3A), they are represented at normal frequency. Some homozygous mutant neonates are notably jaundiced (Fig. 3B), with low hematocrit and birth weight. Many of these pups fail to thrive and die within the first 2 weeks after birth. In addition, most mice that are runted at weaning were determined to be *Ank1*^{E924X} homozygous by PCR genotyping; however, not all *Ank1*^{E924X} homozygous mice are visibly jaundiced at birth or obviously runted at weaning. Analysis of homozygous mutant adult mice (6–10 weeks) revealed that they are severely anemic (hematocrit = 0.22; SD = 0.02) compared to WT littermates (hematocrit = 0.52; SD = 0.03, $p << 0.05$) and the PB red cell fraction consists primarily of reticulocytes (81%) (Fig. 3C). Examination of the PB smears of homozygous mice demonstrated increased polychromasia, amorphous red cells, and increased presence of red cell fragments and nucleated red cells (Fig. 3D). SEM of fixed erythrocytes from WT and homozygous mice revealed amorphous spherical morphology in mutant cells (Fig. 3E). Homozygous mutants that survive weaning have a mean lifespan of 28 weeks (SD = 9). Adult *E924X/E924X* mice (8–12 weeks) are underweight (22 g; SD = 4) compared to WT littermates (34.6 g; SD = 0.6, $p << 0.05$) and suffer from palpable splenomegaly, with the mass of the spleen accounting (upon analysis at necropsy) for approximately 12% of total body mass (Fig. 4A, left panel). In addition to these features, *Ank1*^{E924X} homozygous mice suffer from an enlarged heart (Fig. 4A, right panel) and frequently have gallstones (Fig. 4A, center panel and inset)—characteristics that are common sequelae of hemolytic HS in human patients [2]. In addition, the BM, spleen, and liver are replete with sites of developing erythroblasts (Fig. 4B). With respect to mature erythroblasts, *E924X/E924X* mice have a higher than 10-fold increase in CD71^{+}Ter119^{+} blasts in PB, double the number in the BM, and a 25-fold increase in the spleen (Fig. 5A). We next enumerated the erythroid progenitor populations in these tissues and found that *E924X/E924X* mice have a fourfold increase in the frequency of CFU-E in the BM and a 125-fold increase in the spleen compared to age- and sex-matched WT controls (Fig. 5B). The total CFU-C in the BM is reduced, with the CFU–granulocyte-macrophage and CFU-macrophage progenitor compartments being the most severely affected (Fig. 5B). Although we found approximately half the number of burst-forming unit-erythroid in the BM of homozygous mutant mice, this difference did not reach statistical significance ($p = 0.054$). The apparent myelodysplasia of the BM leads to compensatory extramedullary myelopoiesis, as evidenced by a dramatic increase in CFU-C progenitors detected in the spleen and liver of homozygous *Ank1*^{E924X} mice (Fig. 5B).

Ank1^{E924X} homozygous RBCs express a truncated ankyrin-1 product

Because the *Ank1*^{nb} mutation results in hypomorphic expression of a truncated ankyrin-1 product [17] and the *Ank1*$^{RBC2/RBC2}$ mouse is purportedly functionally ankyrin-null [31], we next attempted to determine whether a stable ankyrin-1 protein is present in *Ank1*^{E924X} RBC ghosts. The theoretical protein product of the *Ank1*^{E924X} allele, barring nonsense-mediated decay of the transcript, should contain only a band 3-binding domain and a severely truncated, presumably nonfunctional, spectrin-binding domain, because E924 is 38 residues N-terminal to the spectrin-binding ZU5 subdomain [8,20,22,24]. The C-terminal regulatory domain should be completely deleted in the protein product of an *Ank1*^{E924X} transcript. Coomassie Blue and immunoblotting analysis of fractionated erythrocyte membrane ghosts prepared from *Ank1*^{E924X} homozygotes revealed an atypical pattern of membrane proteins compared to ghosts prepared from WT (+/+) or Ank1$^{E924X/+}$ littermates (Fig. 6A–C). Many of the major protein bands expected in erythrocyte ghosts are present (Fig. 6A), but also prominent are several equally intensely staining unidentified bands. We surmised that these bands are fragments of various submembranous cytoskeleton components. Importantly, neither a band of the expected size of ankyrin-1 nor protein 4.2 can be identified by Coomassie stain, although ankyrin is typically hard to resolve from spectrin by this method (Fig. 6A). However, using a specific monoclonal antibody to ankyrin-1 (clone 8C3), we detect a cross-reactive band at approximately 100 kDa and, more faintly, at 60 kDa (Fig. 6B). However, we were unable to detect a band that comigrates with full-length ankyrin-1 in *E924X/E924X* RBC ghosts (Fig. 6B). The calculated molecular weight of a truncated ankyrin protein produced from a theoretical *Ank1*^{E924X} transcript is 94.5 kDa. Thus, the 100-kDa band in the *E924X/E924X* lane is a reasonable candidate for an *E924X* truncated protein product. Conversely, although we were not surprised to find a band of similar size in heterozygous *Ank1*^{E924X} mice (albeit at reduced intensity), we were surprised to find a similar band in RBC ghosts prepared from WT littermates.

Using specific antibodies to other components of the band 3–containing RBC protein complexes, we found that, consistent with the *nb/nb* and *RBC2/RBC2* mouse strains and human clinical cases with a hypomorphic *ANK1* expression [2,5], the stability of the full-length forms of proteins in the band 3 macrocomplex (e.g., α-spectrin) and the junctional complex (e.g., β-adducin and actin) are severely affected, such that *E924X/E924X* RBC ghost preparations have much lower concentrations of the proteins of these complex components (Fig. 6C).

Ank1^{E924X} homozygous RBC ghosts contain unique ankyrin-1 protein forms

To our knowledge, the epitope of the α-ankyrin monoclonal antibody 8C3 has not been precisely mapped, but it appears to recognize ankyrin-1 within in the first N-terminal half (1–1012 aa) of the protein [32] and may be expected to recognize an *Ank1* polypeptide truncated at residue 924 (Fig. 7A). However, to further investigate the identity of potential ankyrin-1 products of the *Ank1*^{E924X} mutant allele, we probed RBC ghost preparations with antibodies raised to peptides identical to specific ankyrin-1 domains, including the N-terminus (p89), central spectrin-binding domain (p65), and the translated products of canonical (α-C-term [B]) and alternatively spliced *Ank1* 3′ exons (α-C-term [A&C]) [16,17] (see Fig. 7A). Using the N-terminal ankyrin-1 antibody (p89), we were able to detect a 50-kD and a 100-kD band in *Ank1*$^{E924X/E924X}$ ghosts similar in size to the band detected using 8C3, but only a very faint band of a size consistent with full-length ankyrin-1 (200–210 kD) (Fig. 7Bi). Likewise, this N-terminal ankyrin-1 antibody reacts with a ~100-kD band in the WT lane (Fig. 7Bii). However, only very faint bands of this size were detected by antibodies raised against peptides identical to the spectrin-binding domain (p65) or any of the C-terminal peptide-variants of ankyrin-1—yet these antibodies all recognize bands attributable to full-length ankyrin in the WT lanes. From this result, we can conclude that the

100-kD band in *Ank1*^{E924X} homozygous RBC ghosts is a truncated ankyrin-1 species consisting of an N-terminal band 3-binding domain, but without spectrin-binding and regulatory domains. Because we detected the 100-kD band in both WT and *E924X/E924X* RBC ghosts, this truncated ankyrin form may not be unique to the *Ank1*^{E924X} transcript. We note that the bands detected in the WT lane appear to migrate slightly faster (apparently smaller) than the band detected in the *E924X/E924X* lane (Figs. 6B and 7B). Thus, the truncated ankyrin-1 form in WT RBC ghosts may be distinct from the form in the *E924X/E924X* ghosts. Alternatively, the bands may represent identical polypeptides with different post-translational modifications because the *Ank1*$^{E924X/E924X}$ ghosts are primarily derived from reticulocytes. Notably, a band consistent with the size of a full-length ankyrin-1 appears to be present in homozygous *Ank1*^{E924X} RBC ghosts probed with αC-term (A) raised against a peptide identical to an alternative ankyrin-1 product [16] (Fig. 7Bvii). The presence of a putative full-length ankyrin-1 isoform (possibly from stop codon read-through) may be one explanation for faint 200- to 210-kD bands appearing in the mutant lanes probed with p89 and p65. Note that a band of high intensity at about 125 kD reacting with αC-term (A) is present in the WT, but not *E924X* homozygous lane (Fig. 7Bviii) and thus precludes an argument for contamination from the WT lane as an explanation for the apparently full-sized ankyrin product in the homozygous mutant RBC ghosts. However, we cannot rule out nonspecific cross-reactivity as an alternative explanation. Finally, probing with the C-terminal specific antibodies shows that *Ank1*^{E924X} homozygous mice have a unique pattern of expression (or stabilization) of short forms of *Ank1* (Fig. 7Bvi, ix, xi) that may arise from the known alternative start site in intron 39 [12] coupled with alterative splicing in 3′ exons. The *Ank1*^{E924X} mutation is not expected to directly affect transcription from this alternative start site, and thus the canonical short ankyrin product would not be altered. Notably, other short forms of Ank1 are preferentially expressed or stabilized in homozygous *Ank1*^{E924X} RBC ghosts (Fig. 7Bix, xi).

Discussion

Using ENU random mutagenesis, we have generated a novel mouse model of HS. HS patients with mild to severe forms have slight reticulocytosis and spherocytosis, mild splenomegaly, and minor increase in osmotic fragility but are not anemic. In contrast, patients with severe HS have life-threatening anemia, reticulocytosis, require splenectomy, have increased spherocytosis and osmotic fragility, jaundice, gallstones, and cardiovascular disease [2]. Mice heterozygous for the *Ank1*^{E924X} mutant allele have a phenotype that closely resembles a dominantly inherited, clinically mild human HS. *Ank1*$^{E924X/+}$ mice presented with elevated RBC, decreased MCV, but were normal for all other hematologic values, including hematocrit. *Ank1*$^{E924X/+}$ mice demonstrate slight reticulocytosis, mild splenomegaly, and spherocytosis and a minor increase in osmotic fragility. At the progenitor level, the BM progenitors are normal; however, a sharp increase in CFU-E are observed in the spleen of *Ank1*$^{E924X/+}$ mice, which likely accounts for the elevated RBC. Viable homozygous *Ank1*$^{E924X/E924X}$ mice have the classic severe HS features described here, including severe anemia, in which RBC, hemoglobin, and hematocrit are dramatically reduced.

Mutations in human *ANK1* are a common genetic cause of human HS and several cases have been mapped to mutations that would result in truncation of the spectrin binding and regulatory domains, or even more severe truncation sites within the band 3-binding domain [4]. In fact, point mutations and deletions in human *ANK1* at a position analogous to *Ank1*^{E924X} have previously been described for several HS patients, and frame-shift and nonsense/null mutations are common in dominantly inherited HS [4,5] (see Fig. 2C for examples). In many cases, the human mutant *ANK1* alleles are hypomorphic—but this is often adequately (or fully) compensated by expression from the WT *ANK1* allele [5,33].

Ankyrin-1 haploinsufficiency results in reduced expression or stability of other membrane structural components, including band 3 and the spectrins [2,33]. Although some cases of recessive inheritance have been reported, de novo or dominantly inherited *Ank1* HS are much more common. This is presumably because a functionally ankyrin-null genotype would be lethal.

A spontaneously arising mouse *Ank1* mutation and the resulting normoblastic RBC phenotype in the homozygous-mutant mouse has been described (*nb* mouse) previously [17,34]. The responsible guanosine deletion in *Ank1* exon 38 (transcript variant 1) causes a frame-shift, with a premature termination 13 codons downstream of the base deletion [17]. Although originally thought to be null for ankyrin-1 because of a paucity of *Ank1* message and undetectable ankyrin-1 protein in RBC ghosts [17,35], further analysis revealed that, in fact, red cells of *nb/nb* mice contain low concentrations of a detectable truncated protein product (157 kD) consisting of the N-terminal band 3-binding domain and a central spectrin-binding domain [17] (Fig. 2C). Recently, an ENU-generated point mutation (G → C transversion) in a splice acceptor of *Ank1* intron 40/41 has been reported ($Ank1^{RBC2}$) [31]. Mice homozygous for the *RBC2* mutation are viable but display a spherical RBC morphology, hemolytic anemia, and compensatory erythropoiesis similar to the $Ank1^{nb/nb}$ mouse and the surviving hybrid homozygous $Ank1^{E924X}$ strain reported here. Although mice homozygous for the *RBC2* mutant allele have a fivefold increase in $Ank1^{RBC2}$ transcript (in spleen) compared to WT mice, the authors do not detect ankyrin-1 protein in RBC ghosts and conclude that the *RBC2/RBC2* mouse is functionally *Ank1*-null [31]. Although these authors present compelling evidence that the ankyrin-1 protein is absent in mature red cells and erythroid progenitors from the *RBC2/RBC2* mouse, there remains the possibility that low levels of protein are present but undetected. This is particularly possible because exon 41 has several cryptic splice sites and is differentially spliced [16]. Indeed, our initial analysis of the homozygous $Ank1^{E924X}$ red cell ghosts suggested a functionally ankyrin-null mutant, but longer exposure times and the use of multiple ankyrin antibodies revealed the presence of putative ankyrin isoforms or degraded ankyrin products that may contribute to the survival of mice. Conclusive evidence for the survival of an ankyrin-null mouse model will require a more direct approach, such as a conditional gene deletion.

The phenotype of mice homozygous for the $Ank1^{E924X}$ mutation described in this article resembles severe hemolytic HS in humans. On either a *C3H/HeJ* (N8–9) or *SvImJ/129* (N6) inbred genetic background, the $Ank1^{E924X}$ mutation is lethal late in gestation because live-born homozygous mice were not observed. However, on a mixed *C3H:129* (N2) hybrid strain, homozygous mutant mice were viable but with severe abnormalities due to RBC membrane destabilization and secondary pathologies associated with chronic compensatory extramedullary hematopoiesis, stress erythropoiesis, and chronic hemolysis. Using ankyrin-1 domain-specific antibodies and antibodies to splice variants of ankyrin-1, we detected low-level expression of immunoreactive bands in RBC ghosts prepared from $Ank1^{E924X}$ homozygous mice. Although the novel immunoreactive bands may represent nonspecific cross-reactivity, they may represent degradation products or novel splicing products. The phenotypic analysis of the heterozygous and homozygous animals strongly suggests that the $Ank1^{E924X}$ allele is a loss of function mutation. However, we do not have direct evidence that can rule out the possibility that some truncated peptides may have dominant-negative effects. One prominent band of approximately 100 kD is consistent with the size of the theoretical truncated ankyrin-1 product of the $Ank1^{E924X}$ allele, and other bands are consistent with either rare full-length forms of ankyrin (perhaps from stop codon read-through) or, short forms of *Ank1* normally expressed in skeletal muscle (Fig. 7B). Because transcription of *Ank1* occurs at several known alternative start sites and there are numerous alternative splicing events [11,12,14,16,17], the 100-kD band detected in WT and $Ank1^{E924X}$ heterozygous RBC ghosts could represent the product of one of these forms that,

coincidently, migrates with a size consistent with a *Ank1*^{E924X}-specific theoretical product. If true, the 100-kDa product may result from an alternatively spliced variant of ankyrin-1 that is preferentially translated in mice deficient in functional, full-length ankyrin-1. Although some of the reactive bands we observe could simply be nonspecific cross-reactivity, there remains the possibility that distinct, low-frequency variants of a full-length ankyrin-1 protein are being produced in the homozygous mutant, and that these forms might support survival of the mice. Thus, it is critical to analyze polypeptide products of mutations with multiple antibodies (when available), whether in patients or model organisms, particularly in cases in which the gene is highly regulated at the post-transcriptional level, such as Ank1.

In summary, using an unbiased random mutagenesis approach, we have generated a model of HS that phenocopies mild and severe human HS and several aspects of other hemolytic anemias. We anticipate that the *Ank1*^{E924X} mouse model, especially when comparatively examined with the other mutants in this allelic series (*nb/nb* and *RBC2/RBC2*), will contribute to the understanding of HS genetics and the molecular mechanisms regulating the assembly, stability, and functions of ankyrin-dependent RBC membrane-cytoskeleton complexes. In addition, these models may benefit the study of diseases that develop secondary to chronic hemolysis. As others have shown, *Ank1*-mutant mice have intriguing resistance to malaria parasites [31,36] and a comparative study of the infectivity and pathogenesis of malaria parasites using all three *Ank1* mutant models may provide mechanistic insights into malaria virulence and the genetics of human susceptibility. Importantly, comparative studies of any typewill require that the various mutant *Ank1* alleles be bred to identical mouse strains. To this end, having the *Ank1*^{E924X} allele already on the *C3H/HeJ* and *SvImJ/129* strains, we are backcrossing to the *C57Bl/6* and *Balb/c* backgrounds in anticipation of studies that will allow direct mechanistic comparisons of these mouse models of human disease.

Supplementary Material

Refer to Web version on PubMed Central for supplementary material.

Acknowledgments

We thank Dr. Mark Scott, Wendy Toyofuku, and Dr. Dana Devine (UBC Centre for Blood Research and Canadian Blood Services) for access to automated blood analyzer instruments and technical assistance, Takahide Murakami for PCR genotyping, Krista Ranta and Matthew Cowan and The Biomedical Research Centre transgenic core staff for animal care support and Derrick Horne for technical assistance with electron microscopy. The authors wish to thank Genome BC (Vancouver, BC) for providing DNA sequencing support at cost recovery rates. M.R.H. and S.M. are fellows of the Canadian Institutes of Health Research (CIHR)/Heart & Stroke Foundation of Canada (HSFC) Strategic Training Program in Transfusion Science at the UBC Centre for Blood Research (CBR) and M.R.H. is a recipient of a HSFC Junior Personnel Fellowship. N.A. was supported by the Dina Gordon Malkin Ontario Graduate Scholarship in Science & Technology and a Heart & Stroke/Richard Lewar Centre of Excellence Scholarship. J.W. was supported by a Canadian Stem Cell Network Co-op Award. C.S.B. and L.L.P. were supported by National Institutes of Health (Bethesda, MD, USA) grant HL088468 (L.L.P.). K.M.M. is a Michael Smith Foundation for Health Research Senior Scholar and CBR member. This study was funded by a group operating grant from the CIHR (FRN 74611) to D.L.B., R.P., C.W., M.D.M., K.M.M., and W.L.S. (leader), a CIHR grant to K.M.M. (MOP-93580), and a grant from the Heart and Stroke Foundation of Ontario (NA-6363) (W.L.S.). W.L.S. is supported by a Canada Research Chair.

References

1. Flenniken AM, Osborne LR, Anderson N, et al. A Gja1 missense mutation in a mouse model of oculodentodigital dysplasia. Development. 2005; 132:4375–4386. [PubMed: 16155213]
2. Perrotta S, Gallagher P, Mohandas N. Hereditary spherocytosis. Lancet. 2008; 372:1411–1426. [PubMed: 18940465]

3. Sato T, Vries R, Snippert H, et al. Single Lgr5 stem cells build crypt-villus structures in vitro without a mesenchymal niche. Nature. 2009; 459:262–265. [PubMed: 19329995]
4. Gallagher P. Hematologically important mutations: ankyrin variants in hereditary spherocytosis. Blood Cells Mol Dis. 2005; 35:345–347. [PubMed: 16223590]
5. Eber SW, Gonzalez JM, Lux ML, et al. Ankyrin-1 mutations are a major cause of dominant and recessive hereditary spherocytosis. Nat Genet. 1996; 13:214–218. [PubMed: 8640229]
6. Eber S, Lux SE. Hereditary spherocytosis–defects in proteins that connect the membrane skeleton to the lipid bilayer. Semin Hematol. 2004; 41:118–141. [PubMed: 15071790]
7. Bennett V, Healy J. Organizing the fluid membrane bilayer: diseases linked to spectrin and ankyrin. Trends Mol Med. 2008; 14:28–36. [PubMed: 18083066]
8. Bennett V. Purification of an active proteolytic fragment of the membrane attachment site for human erythrocyte spectrin. J Biol Chem. 1978; 253:2292–2299. [PubMed: 632270]
9. Peters L, Birkenmeier C, Bronson R, et al. Purkinje cell degeneration associated with erythroid ankyrin deficiency in nb/nb mice. J Cell Biol. 1991; 114:1233–1241. [PubMed: 1716634]
10. Kordeli E, Bennett V. Distinct ankyrin isoforms at neuron cell bodies and nodes of Ranvier resolved using erythrocyte ankyrin-deficient mice. J Cell Biol. 1991; 114:1243–1259. [PubMed: 1832678]
11. Zhou D, Birkenmeier CS, Williams MW, Sharp JJ, Barker JE, Bloch RJ. Small, membrane-bound, alternatively spliced forms of ankyrin 1 associated with the sarcoplasmic reticulum of mammalian skeletal muscle. J Cell Biol. 1997; 136:621–631. [PubMed: 9024692]
12. Birkenmeier C, Sharp J, Gifford E, Deveau S, Barker J. An alternative first exon in the distal end of the erythroid ankyrin gene leads to production of a small isoform containing an NH2-terminal membrane anchor. Genomics. 1998; 50:79–88. [PubMed: 9628825]
13. Gallagher PG, Forget BG. An alternate promoter directs expression of a truncated, muscle-specific isoform of the human ankyrin 1 gene. J Biol Chem. 1998; 273:1339–1348. [PubMed: 9430667]
14. Peters LL, Turtzo LC, Birkenmeier CS, Barker JE. Distinct fetal Ank-1 and Ank-2 related proteins and mRNAs in normal and nb/nb mice. Blood. 1993; 81:2144–2149. [PubMed: 8471772]
15. Gallagher P, Tse W, Scarpa A, Lux S, Forget B. Structure and organization of the human ankyrin-1 gene. Basis for complexity of pre-mRNA processing. J Biol Chem. 1997; 272:19220–19228. [PubMed: 9235914]
16. Birkenmeier CS, White RA, Peters LL, Hall EJ, Lux SE, Barker JE. Complex patterns of sequence variation and multiple 5' and 3' ends are found among transcripts of the erythroid ankyrin gene. J Biol Chem. 1993; 268:9533–9540. [PubMed: 8486643]
17. Birkenmeier C, Gifford E, Barker J. Normoblastosis, a murine model for ankyrin-deficient hemolytic anemia, is caused by a hypomorphic mutation in the erythroid ankyrin gene Ank1. Hematol J. 2003; 4:445–449. [PubMed: 14671619]
18. Porter NC, Resneck WG, O'Neill A, Van Rossum DB, Stone MR, Bloch RJ. Association of small ankyrin 1 with the sarcoplasmic reticulum. Mol Membr Biol. 2005; 22:421–432. [PubMed: 16308276]
19. Rubtsov AM, Lopina OD. Ankyrins. FEBS Lett. 2000; 482:1–5. [PubMed: 11018513]
20. Ding Y, Kobayashi S, Kopito R. Mapping of ankyrin binding determinants on the erythroid anion exchanger, AE1. J Biol Chem. 1996; 271:22494–22498. [PubMed: 8798415]
21. Czogalla A, Jaszewski AR, Diakowski W, Bok E, Jezierski A, Sikorski AF. Structural insight into an ankyrin-sensitive lipid-binding site of erythroid beta-spectrin. Mol Membr Biol. 2007; 24:215–224. [PubMed: 17520478]
22. Ipsaro J, Huang L. Mondrag[notdef]on A. Structures of the spectrin-ankyrin interaction binding domains. Blood. 2009; 113:5385–5393. [PubMed: 19141864]
23. Stabach P, Simonovic I, Ranieri M, et al. The structure of the ankyrin-binding site of β-spectrin reveals how tandem spectrin-repeats generate unique ligand-binding properties. Blood. 2009; 113:5377–5384. [PubMed: 19168783]
24. Kodippili GC, Spector J, Sullivan C, et al. Imaging of the diffusion of single band 3 molecules on normal and mutant erythrocytes. Blood. 2009; 113:6237–6245. [PubMed: 19369229]

25. Hall TG, Bennett V. Regulatory domains of erythrocyte ankyrin. J Biol Chem. 1987; 262:10537–10545. [PubMed: 3038887]
26. Davis LH, Davis JQ, Bennett V. Ankyrin regulation: an alternatively spliced segment of the regulatory domain functions as an intramolecular modulator. J Biol Chem. 1992; 267:18966–18972. [PubMed: 1388161]
27. Pao-Wen L, Chu-Jing S, Mariano T. Phosphorylation of ankyrin decreases its affinity for spectrin tetramer. J Biol Chem. 1987; 60:14958–14964.
28. Gallagher PG, Tse WT, Scarpa AL, Lux SE, Forget BG. Large numbers of alternatively spliced isoforms of the regulatory region of human erythrocyte ankyrin. Trans Assoc Am Physicians. 1992; 105:268–277. [PubMed: 1309004]
29. Justice MJ, Carpenter DA, Favor J, et al. Effects of ENU dosage on mouse strains. Mamm Genome. 2000; 11:484–488. [PubMed: 10886010]
30. Girodon F, Garcon L, Bergoin E, et al. Usefulness of the eosin-5'-maleimide cytometric method as a first-line screening test for the diagnosis of hereditary spherocytosis: comparison with ektacytometry and protein electrophoresis. Br J Haematol. 2008; 140:468–470. [PubMed: 18162119]
31. Rank G, Sutton R, Marshall V, et al. Novel roles for erythroid Ankyrin-1 revealed through an ENU-induced null mouse mutant. Blood. 2009; 113:3352–3362. [PubMed: 19179303]
32. Raphael P, Takakuwa Y, Manno S, Liu SC, Chishti AH, Hanspal M. A cysteine protease activity from Plasmodium falciparum cleaves human erythrocyte ankyrin. Mol Biochem Parasitol. 2000; 110:259–272. [PubMed: 11071281]
33. Ozcan R, Jarolim P, Lux SE, Ungewickell E, Eber SW. Simultaneous (AC)n microsatellite polymorphism analysis and single-stranded conformation polymorphism screening is an efficient strategy for detecting ankyrin-1 mutations in dominant hereditary spherocytosis. Br J Haematol. 2003; 122:669–677. [PubMed: 12899723]
34. Bernstein SE. Hereditary disorders of the rodent erythron. In: Anonymous Genetics in Laboratory Animal Medicine: Proceedings of a Symposium Conducted at Boston, Massachusetts, July 22, 1968. National Academy of Sciences. 1969; 9
35. Bodine DM 4th, Birkenmeier CS, Barker JE. Spectrin deficient inherited hemolytic anemias in the mouse: characterization by spectrin synthesis and mRNA activity in reticulocytes. Cell. 1984; 37:721–729. [PubMed: 6234993]
36. Shear HL, Roth EF Jr, Ng C, Nagel RL. Resistance to malaria in ankyrin and spectrin deficient mice. Br J Haematol. 1991; 78:555–560. [PubMed: 1832936]
37. Ito CY, Li CY, Bernstein A, Dick JE, Stanford WL. Hematopoietic stem cell and progenitor defects in Sca-1/Ly-6A-null mice. Blood. 2003; 101:517–523. [PubMed: 12393491]

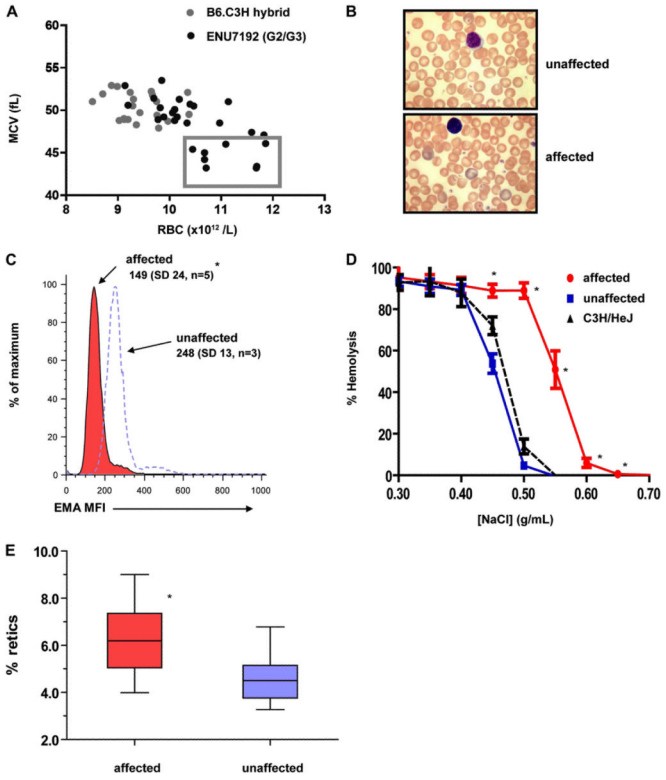

Figure 1.

The RBC phenotype of an ENU-generated mutant mouse strain *ENU7192* demonstrates diagnostic features of human hereditary spherocytosis. (**A**) Enumeration and MCV of RBC parameters of individual mice from a *B6.C3H* control hybrid strain (gray) and generation 2 and 3 (G2/3) progeny of mutagenized strain *ENU7192* (black). Individual affected mice with RBC count and MCV parameters deviating by more than 2 SDs (box) from nonaffected littermates and nonmutagenized hybrid controls were selected for heritability testing and mapping. (**B**) Wright-Geimsa stain of PB smear of unaffected (upper panel) and affected (lower panel) ENU7192 at 400× magnification. (**C**) Histogram of mean fluorescence intensity (MFI) of RBCs labeled with eosin-5′-maleimide (EMA) where affected (red) and nonaffected (open peak) mice are defined by the low MCV parameter and confirmed by prospective PCR genotyping for the *E924X* or WT *Ank1* genotypes (see Supplementary Figure E1; online only, available at www.exphem.org). The mean MFI values and SDs are shown. (**D**) Osmotic hemolysis plot of RBCs from affected (● red) and nonaffected (■ blue) *ENU7192* (C3H N8–9) mice and C3H/HeJ parental strain (▲ black, dashed lined) (n = 4–7 mice per strain). (**E**) Affected mice (red) have increased percent of circulating reticulocytes compared to nonaffected littermates (blue). *Significantly different than unaffected mice with $p < 0.05$.

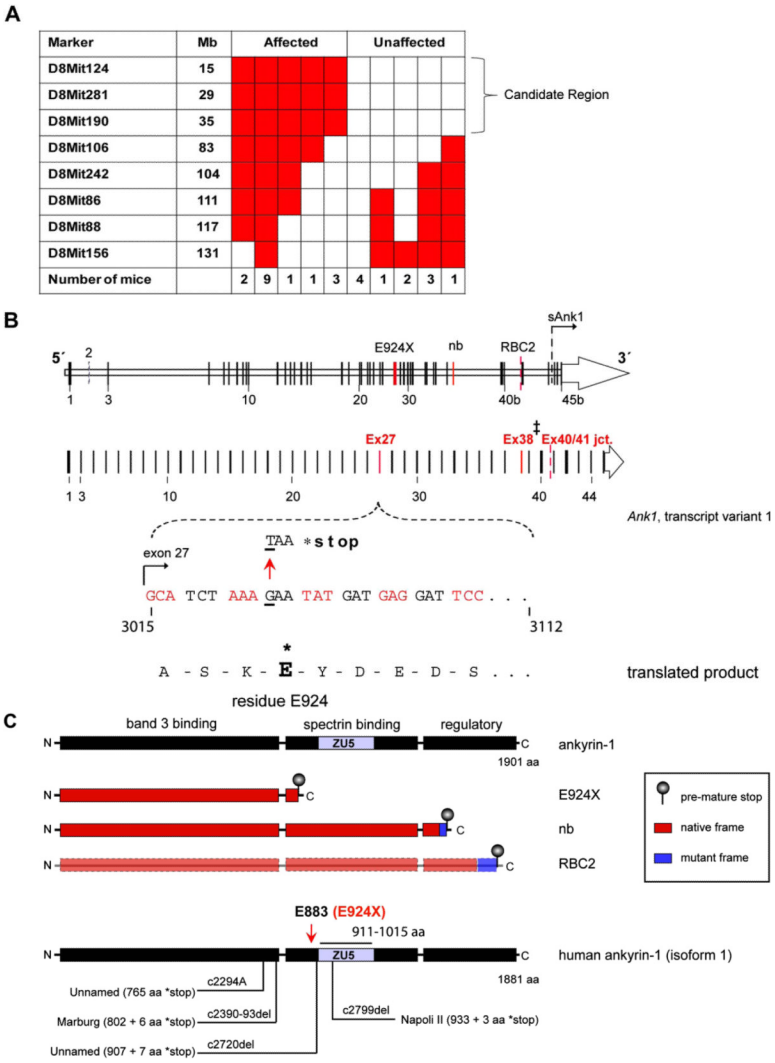

Figure 2.

A single ENU-generated point mutation (G → T transversion) in *Ank1* exon 27 yields a new mouse model of hereditary spherocytosis. (**A**) Table indicating the number of affected and unaffected *ENU7192* mice heterozygous (red) or null (white) for Chr. 8 marker loci derived from the mutagenized strain (B6). The indicated candidate region of Chr. 8 indicated is linked to the mutant phenotype of affected mice. (**B**) Schematic mouse *Ank1* locus highlight transcript variant 1 and the mapped position of the *ENU7192* point mutation (in *Ank1*). A portion of *Ank1* exon 27 is expanded to show the genomic sequence with the position of the ENU-generated point mutation (G → T transversion) encoding a stop codon (*) in place of glutamate (E) at residue 924 (ankyrin-1, isoform 1 [NP001104253.1]) of the theoretical translated product. The locations of the E924X point mutation within the *Ank1* genomic locus relative to other reported *Ank1* mutant mouse strains ($Ank1^{nb}$ (nb) [17] and $Ank1^{RBC2}$ (RBC2) [31]) is shown. ‡Note that the *nb* mutation is in exon 38 using the exon numbering for *Ank1*, transcript variant 1(NM001110783.1) but is reported as exon 36 in the original mapping publication [17]). s*Ank1* indicates the position of the alternative start site for the short ankyrin-1 isoform using the exon numbering scheme of *Ank1*, transcript variant 1 [12]. (**C**) The theoretical truncated ankyrin-1 protein products generated by the known *Ank1* mouse mutant alleles. Note that ankyrin-1 protein attributable to the *RBC2* allele has not been detected in reticulocytes or erythroid progenitors [31].

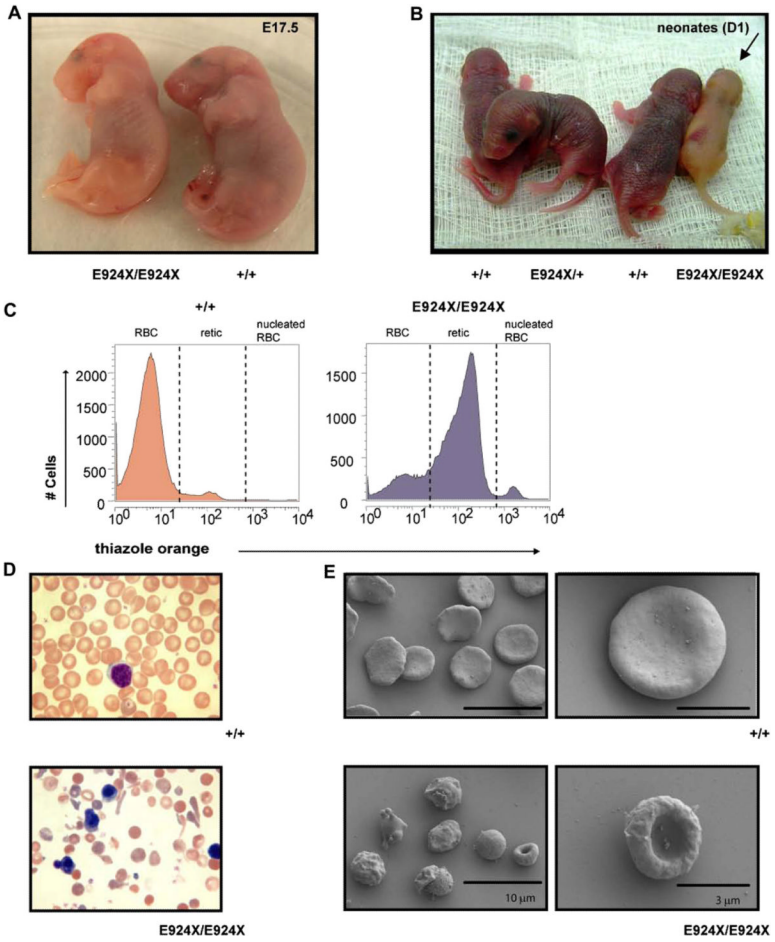

Figure 3.

Homozygous *Ank1*^{E924X} mice display severe, hemolytic anemia and RBC structural defects. (**A**) E17.5 embryos and (**B**) day 1 neonates obtained from *Ank1*$^{E924X/+}$ intercross matings of a hybrid strain (C3J;129 [N2]). The *Ank1*^{E924X} genotype abbreviations are as indicated for wild-type (+/+), heterozygous (*E924X*/+), or homozygous mutants (*E924X/E924X*). The arrow indicates a jaundiced pup. (**C**) Flow cytometric analysis histograms of thiazole orange–stained PB collected from WT (+/+) and *E924X/E924X* mice. Cells were first gated for forward scatter (FSC) and side scatter (SSC) properties on a log-scale to exclude platelets and white blood cells from the analysis. The peak in the third decade includes nucleated erythroblasts present in the PB of *E924X/E924X* mice and these were excluded from the retic % calculation. There is no significant contribution of nucleated erythroblasts in the analysis of WT mice. (**D**) Wright-Geimsa stains of PB smears of WT (+/+) (upper panel) and *Ank1*^{E924X} homozygous mutant mice (lower panel) at 400× magnification. (**E**) Scanning electron micrographs (SEM) (HitachiS4700 FESEM at 2 kV) of fixed red cells sampled from +/+ (upper panels) and *E924X/E924X* (lower panels). Scale bars for SEM: 10 μm (left panels) and 3 μm (right panels). Micrographs and photographs were processed in Adobe Illustrator (11.0) with equal scaling and color correction (where appropriate).

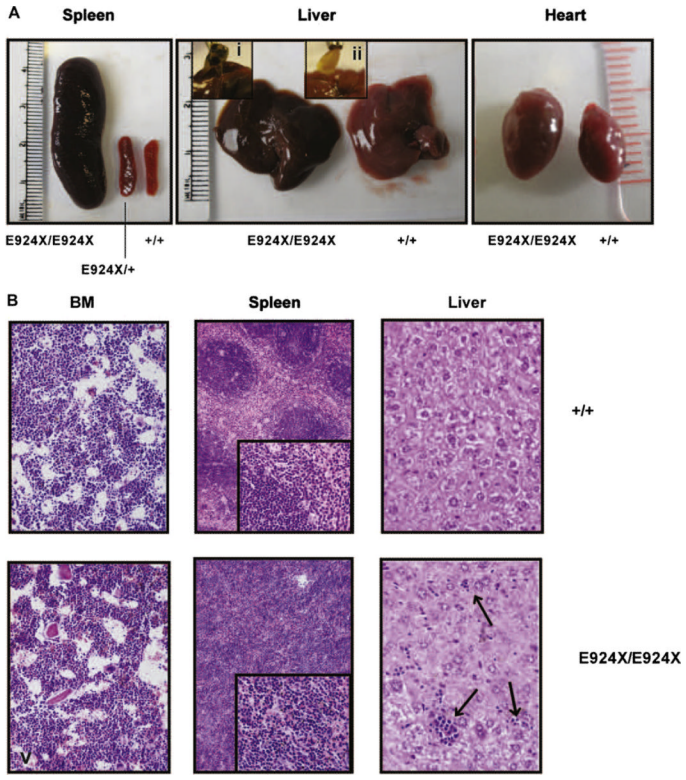

Figure 4.

Ank1^{E924X} homozygous mice display several phenotypes analogous to the pathological features of severe hereditary spherocytosis in humans. (A) Photographs of spleen (left panel), liver (center panel), gall bladder with gallstones (i, ii, inset) and heart (right panel) dissected from 8- to 12-week-old WT (+/+), heterozygous mutant (*E924X*/+) (only spleen shown) and homozygous mutant (*E924X*/*E924X*) mice (*C3H:129* [N2] hybrid). (B) Micrographs of hematoxylin and eosin–stained sections of formalin-fixed BM (400×), spleen (200×, inset 400×). Arrows in the liver sections indicate sites of extramedullary erythropoiesis in the liver (images acquired with Olympus C-5060 digital camera). Photographs and micrographs were processed in Adobe Illustrator (11.0) with equal scaling and color correction where appropriate for presentation.

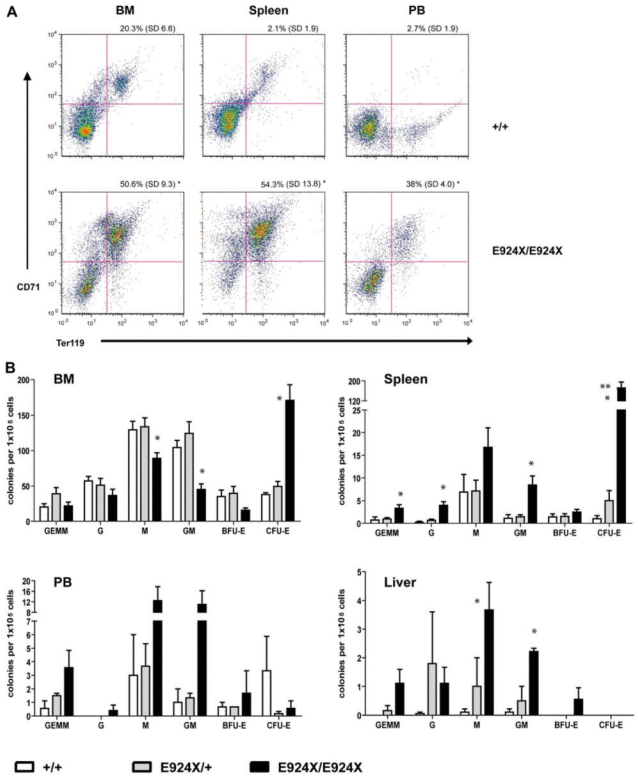

Figure 5.

Ank1^{E924X} homozygous mutant mice demonstrate profound compensatory erythropoiesis in the spleen, liver, and peripheral blood. (A) Representative CD71/Ter119 flow cytometry profiles of BM, spleen, and PB. RBCs were lysed to exclude mature erythrocytes and reticulocytes. The percentage of $CD71^{+}Ter119^{+}$ cells (erythroblasts) (upper right quadrant) as a percentage of total cells for the indicated tissues is shown. (B) CFU-C present (per 1×10^5 nucleated cells plated) in the indicated tissues of WT (+/+) (open bars), *E924X*/+ (shaded bars) and *E924X*/*E924X* (solid bars) mutant mice. *Significantly different than both WT and *E924X*/+ with $p < 0.05$. **Significantly different than *E985X*/+ with $p < 0.05$.

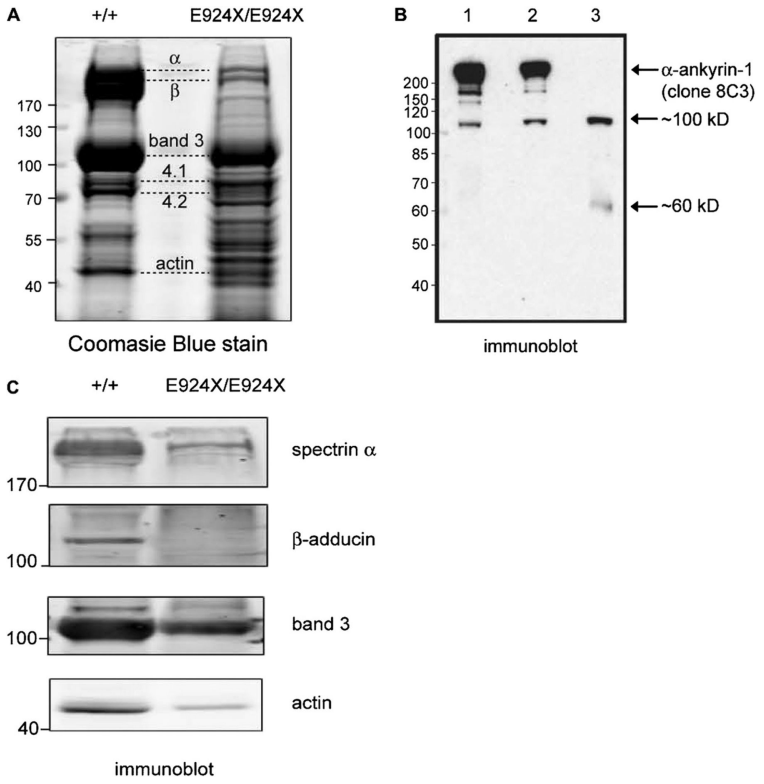

Figure 6.

Several components of the band 3 macrocomplexes are destabilized in *Ank1*^{E924X} homozygous mice. (A) Coomasie Blue stain of fractionated RBC ghosts (10% sodium dodecyl sulfate polyacrylamide gel electrophoresis) prepared from PB of WT (+/+) and homozygous *Ank1*^{E924X} (*E924X*/*E924X*) mutant mice. Positions of the major RBC membrane proteins are indicated with dashed lines. (B) Immunoblot (α– ankyrin-1 monoclonal antibody [clone 8C3]) of fractionated RBC ghosts prepared from (1) WT (+/+), (2) *E924X*/+, and (3) *E924X*/*E924X* blood. Arrows indicate major immunoreactive bands. (C) Immuno-blot of fractionated RBC ghosts prepared from WT (+/+) and *E924X*/*E924X* blood probed with antibodies raised against major RBC membrane and cytoskeletal proteins. For all experiments, gel lanes were loaded with equal concentrations of total protein as measured by BCA assay. The size of molecular weight markers (in kD) and the identification of protein bands are indicated. Digital scans and LI-COR images were processed in Adobe Illustrator (11.0) with equal scaling and contrast enhancement, where required.

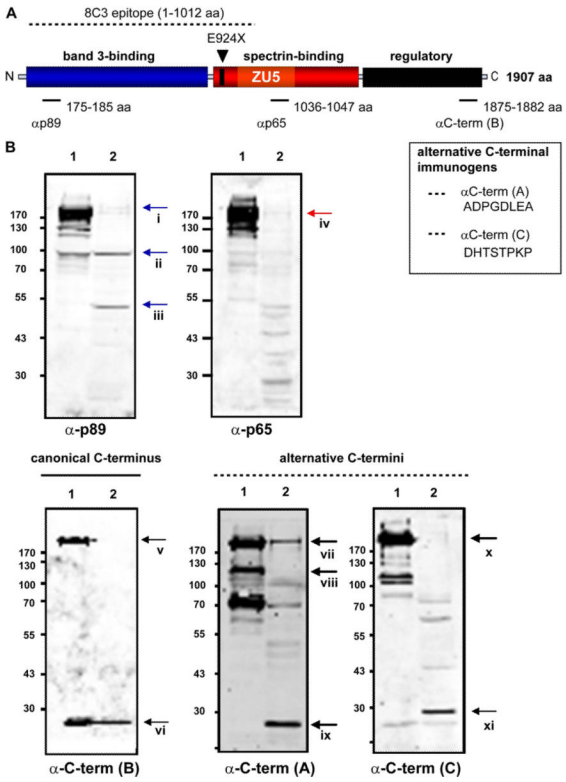

Figure 7.

Ank1^{E924X} homozygous mutant mice express several unique truncated forms of ankyrin. (A) Schematic of the structural domains of erythroid ankyrin protein and the site of the theoretical E924X truncation. Peptides (p89, p65, αC-term [A], [B], and [C]) identical to the indicated residues of the products of canonical (isoforms 1 and 2) and alternatively spliced variants of mouse *Ank1* were used to raise domain-specific antibodies (rabbit primary antibodies). The location of residues (ankyrin 1, isoform 1) of canonical peptides used as immunogens are indicated in the schematic and the alternative C-terminal peptides are shown (inset box). (B) Immunoblots of RBC ghosts prepared from (1) WT (+/+) and (2) *E924X/E924X* mice, fractioned by sodium dodecyl sulfate polyacrylamide gel electrophoresis and probed with ankyrin domain-specific anti-sera as indicated. LI-COR images were processed in Adobe Illustrator (11.0) with equal scaling and contrast enhancement where required.

Table 1

Summary of dominant ENU hematopoiesis screen

		WBC (n)	WBC on smear	RBC (n)	MCV/MCH	RBC multiparameters	Platelets	Multiple lineages
Total number of G1s screened	3392							
No. of G1 outliers	88	24	4	7	30	11	10	2
No. of G1s breed to test heritability	43	10	3	7	9	6	6	2
No. of G1s heritable	17	7	2	0	5	5	5	0
No. of G1s not heritable	23	2	1	7	4	0	1	2
No. of G1s heritable and mapped	11	1	1	0	3	4	3	0

MCH = mean cell hemoglobin; WBC = white blood cell.

Exp Hematol. Author manuscript; available in PMC 2012 July 25.

Table 2

Peripheral blood parameters of *ENU7192* model of hereditary spherocytosis

Strain	**C3H/HeJ (N8–9)**		**Hybrid**		
Phenotype	**Nonaffected**	**Affected**	**Nonaffected**	**Affected**	**Affected**
Genotype	**WT**	***Ank1*** $^{7192/+}$	**WT**	***Ank1*** $^{7192/+}$	***Ank1*** $^{7192/7192}$
No. of mice	19	26	35	50	10
RBC ($\times 10^{12}$/L)	9.6 (0.5)	11.1 (0.8) *	10.2 (0.6)	11.3 (0.7) *	4.0 (0.4) *
Hgb (g/L)	170 (8)	170 (11)	170 (9)	168 (10)	61 (4) *
HCT (ratio)	0.52 (0.03)	0.54 (0.04)	0.52 (0.03)	0.51 (0.04)	0.22 (0.02) *
MCV (fL)	54 (1)	49 (2) *	51 (2)	45 (2) *	56 (3)
MCH (pg)	17.3 (0.4)	15.2 (0.7) *	16.8 (1.0)	14.9 (0.7) *	15.3 (0.9)
MCHC (g/L)	320 (9)	310 (12) *	329 (16)	331 (16)	272 (12) *
PLT ($\times 10^{9}$/L)	1225 (210)	1256 (241)	781 (229)	912 (162)	755 (199)
WBC † ($\times 10^{9}$/L)	10.6 (2.0)	11.9 (2.4)	11.1 ± (3.1)	10.8 ± (2.5)	169 (17.5) *

Values in parentheses are SDs.

HCT = hematocrit; Hgb = hemoglobin; MCHC = mean cell hemoglobin concentration; MCH = mean cell hemoglobin; PLT = platelet; WBC = white blood cell.

* $p << 0.05$.

† The WBC values reflect increases in reticulocytes due to overlapping size of WBC and reticulocytes.